High Resolution Validation in the Shortwave: ASTI/LBLRTM QME

P. D. Brown, S. A. Clough, and E. J. Mlawer
Atmospheric and Environmental Research, Inc.
Cambridge, Massachusetts

T. R. Shippert
Pacific Northwest National Laboratory
Richland, Washington

F. J. Murcray
Denver University
Denver, Colorado

Introduction

To assess our modeling capability in the shortwave and to resolve issues including those described by Cess et al. (1995) and others (Li and Moreau 1996; Arking 1996), a Quality Measurement Experiment (QME) has been initiated that extends the approach of the longwave AERI/LBLRTM (atmospheric emitted radiance interferometer/line by line radiative transfer model) QME (Brown et al. 1998) to shorter wavelengths. This shortwave QME for the clear sky focuses upon three components: 1) the ability to accurately measure downwelling radiance, 2) the capability to model both terrestrial extinction and extraterrestrial radiance, and 3) the ability to accurately characterize the atmospheric state in the radiating column. The initial focus of the QME is upon the spectral region measured by the University of Denver absolute solar transmittance interferometer (ASTI) instrument, from 2000 cm^{-1} to 10000 cm^{-1}. Efforts are underway to extend the analyses to 28600 cm^{-1} using the State University of New York (SUNY) Albany rotating shadowband spectroradiometer (RSS; Harrison et al. 1998). The strategy of this QME is to initially focus upon clear sky, direct beam radiance analyses, and to later extend the study to the total incoming irradiance. Principal areas of focus include errors in the line parameter database, continuum issues, and solar source function accuracy.

Observed Data

The high resolution content of the ASTI spectra provides an excellent dataset for identifying molecular absorption issues, assessing the ability to accurately measure radiation in the solar spectral regime, and evaluating the solar source function. The ASTI instrument is comprised of three filters over the spectral range 2000 cm^{-1} to 10000 cm^{-1} and has a resolution of 0.6 cm^{-1} (HWHM). It measures the downwelling radiance in the direct solar beam, with a field of view (FOV) covering the central 16% of the solar disk (.4 times the disk radius), and is colocated with the AERI instrument at the Southern Great Plains (SGP) central facility (CF) site. It uses a 2800 K tungsten lamp for calibration. A sample ASTI spectrum is shown in Figure 1.

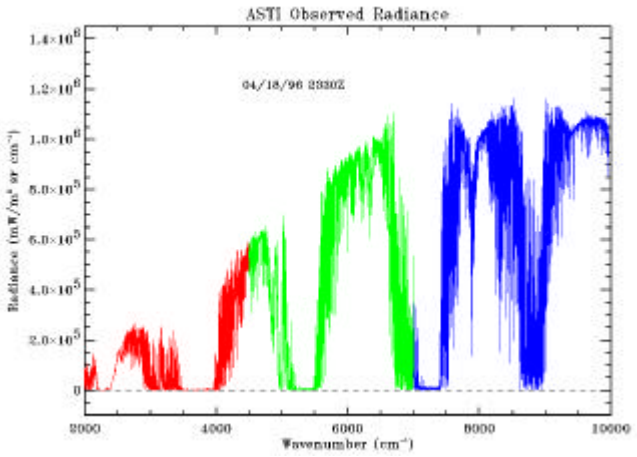

Figure 1. A typical ASTI observed radiance spectrum. The different colors denote the spectral ranges of the three filters. (For a color version of this figure, please see *http://www.arm.gov/docs/documents/technical/conf_9803/brown-98.pdf*.)

Validation Cases

Spectral validations of the ASTI measurements are performed with line-by-line calculations using LBLRTM. Input profiles of atmospheric temperature, ozone, and other trace gases are similar to those of the AERI/LBLRTM QME. Water vapor profiles are obtained by scaling the radiosonde profiles to be consistent in precipitable water column amount with the Atmospheric Radiation Measurement (ARM) microwave radiometer (MWR) measurement at 23.8 GHz. This method is identical to that used in the longwave AERI/LBLRTM QME.

The current analyses focus upon three validation cases ranging in precipitable water vapor from 0.6 cm to 3.3 cm in the vertical path and 27.9° to 71.5° solar zenith angle. Table 1 outlines the atmospheric and temporal states associated with the three cases.

Table 1. The three ASTI cases used in the initial analyses. The table shows the date and time of the observation, the associated precipitable water vapor amount in the vertical column, and the solar zenith angle.

Case #	Date	Time (Z)	H_2O (prec cm)	Solar Zenith (degrees)
1	04/18/96	1730	0.60	31.0
2	04/18/96	2330	0.75	71.5
3	06/24/97	2040	3.30	27.9

Solar Source Function

The solar source function used in the QME is that of Kurucz (1992). It is the result of a radiative transfer calculation based upon solar measurements, with a resolution of 0.004 cm^{-1} at 2000 cm^{-1} and 0.02 cm^{-1} at 10000 cm^{-1}. The spectra have been interpolated to match the spectral sampling of the monochromatic radiance calculation. Figures 2a and 2b show the Kurucz spectrum and that of Neckel and Labs (1984), respectively. The two spectra can be compared directly by degrading the Kurucz spectrum to the resolution of the Neckel and Labs spectrum (10 cm^{-1}). The incoming solar radiance spectrum used to this point is for the full solar disk. Future validations will use an extraterrestrial spectrum from Kurucz computed for the central 16% of the disk.

Spectral Analyses

Prior to implementing the full QME, some processing of the inputs has been required. In particular, the ASTI data has been spectrally calibrated to account for the finite field of view, Rayleigh extinction has been added to the LBLRTM calculation, and two collision-induced O_2 bands have been included in the model. Issues associated with these validations include the solar source function, ASTI photometric calibration, aerosol extinction, the HITRAN linefile database, and the water vapor continuum. Figure 3 shows an ASTI observed spectrum over the spectral range 6300 cm^{-1} to 8200 cm^{-1} taken April 18, 1998, at 2330Z (71.5° solar zenith angle) with an associated water vapor column of 0.75 precipitable centimeters in the vertical

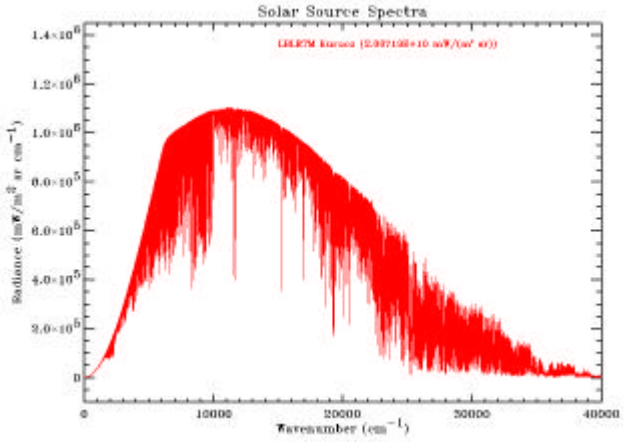

Figure 2a. The Kurucz calculated solar spectrum for the full solar disk. (For a color version of this figure, please see *http://www.arm.gov/docs/documents/technical/conf_9803/brown-98.pdf*.)

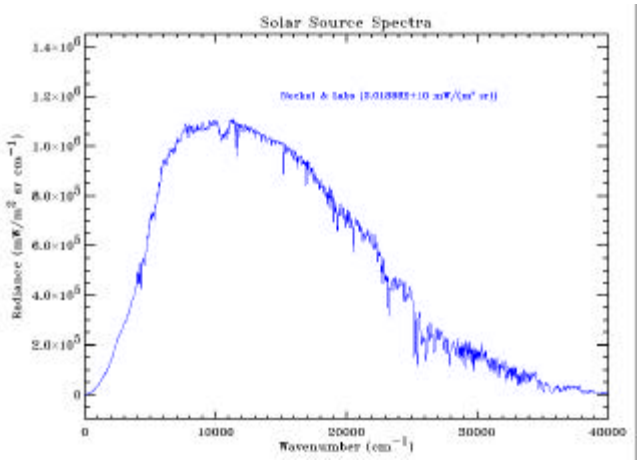

Figure 2b. The Neckel and Labs solar spectrum. (For a color version of this figure, please see *http://www.arm.gov/docs/documents/technical/conf_9803/brown-98.pdf*.)

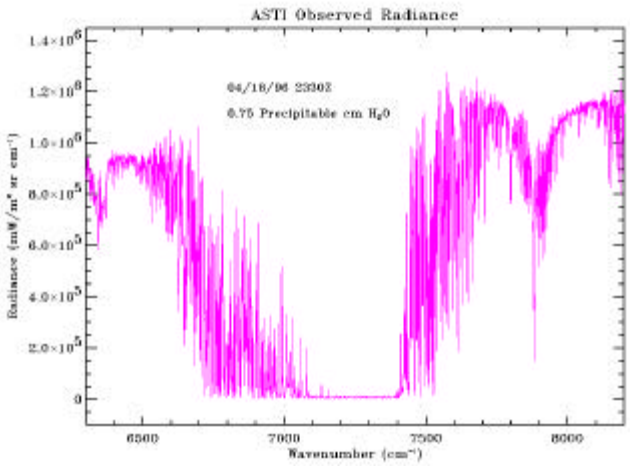

Figure 3. ASTI observation from April 18, 1998. (For a color version of this figure, please see *http://www.arm.gov/docs/documents/technical/conf_9803/brown-98.pdf*.)

column. Residuals between ASTI-observed radiance and the LBLRTM calculation, excluding the spectral calibration, the Rayleigh extinction calculation, and the O_2 band absorption calculation, are shown in the top panel of Figure 4. The large spectral residuals in the regions of 6500 cm^{-1} to 7050 cm^{-1} and 7400 cm^{-1} to 8200 cm^{-1} in the top panel are attributable to the neglect of the finite field of view in modeling the instrument function. The band-like residuals in the 7700 cm^{-1} to 8100 cm^{-1} region result from the absence of the collision induced O_2 band in the model. Aerosol extinction, Rayleigh scattering, and/or ASTI photometric calibration error contribute to the positive offset over the 7500 cm^{-1} to 8200 cm^{-1} region.

To account for the spectral impact of the finite field of view, two factors ??0 and ?d? were applied to the spectral wavenumber function

?i = ?0 + d?*i,

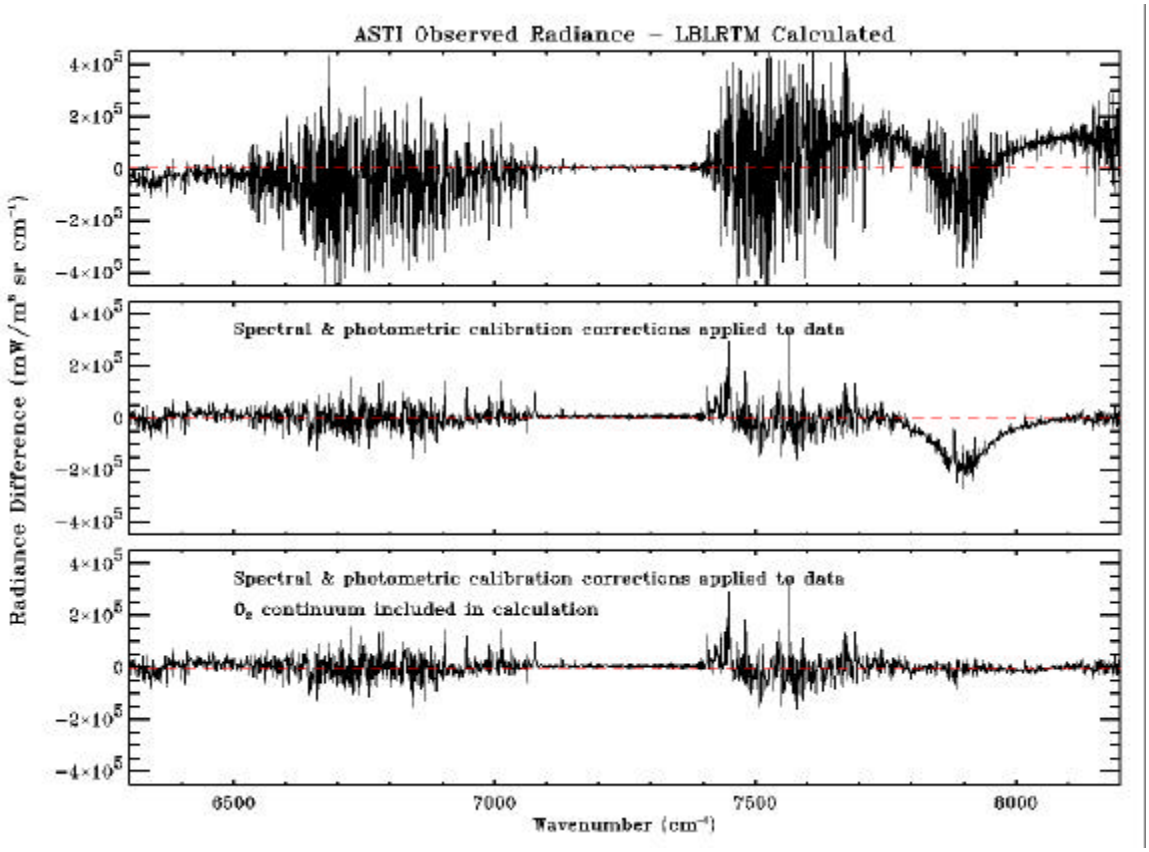

Figure 4. Observed - Calculated residuals neglecting instrument FOV effects in the spectral calibration, Rayleigh extinction, and O_2 collision induced absorption (top); excluding only O_2 collision induced absorption (center); and including instrument FOV effects in the spectral calibration, Rayleigh extinction, and O_2 collision induced absorption (bottom). (For a color version of this figure, please see *http://www.arm.gov/docs/documents/technical/conf_9803/brown-98.pdf*.)

where i is the i^{th} element of the spectral array. This yields a new spectral wavenumber function

?i = (?0 + ??0) + (d??????d??*i).

To separate the effects of high spectral content from those with lower spectral content, the ASTI radiances have been scaled to the Kurucz solar source function in the transparent window regions for selected spectral domains. A total of six scale factors, obtained from the windows 2140 cm^{-1} to 2145 cm^{-1}, 2657 cm^{-1} to 2660 cm^{-1}, 4665 cm^{-1} to 4695 cm^{-1}, 6425 cm^{-1} to 6435 cm^{-1}, 8050 cm^{-1} to 8080 cm^{-1}, and 9700 cm^{-1} to 9730 cm^{-1}, are applied over the ASTI region of spectral coverage. The scale factors correct for the effects of aerosol extinction, Rayleigh scattering, ASTI calibration error, and errors associated with the solar source function. The effects of Rayleigh scattering are well understood; the extinction due to Rayleigh scattering has been implemented in the LBLRTM model. Aerosol extinction will be obtained from the analyses of the multifilter rotating shadowband radiometer (MFRSR; Harrison et al. 1994) and will be included in the calculation. The greatest challenge will be to distinguish between the effects of photometric calibration error and potential issues associated with the Kurucz solar source function. The center panel of Figure 4 shows the residuals after correcting for the finite field of view and applying the scale factor in the region 8050 cm^{-1} to 8080 cm^{-1}.

A formulation of the O_2 continuum has been added to LBLRTM by Mlawer et al. (1998) based upon these shortwave measurements. The bottom panel of Figure 4 shows the residuals between the ASTI measurement and the LBLRTM model, which includes the O_2 continuum in the 7874 cm^{-1} band. Another band of O_2 centered at 9434 cm^{-1} has also been modeled, and a third band at 6329 cm^{-1} has been identified, but has not been modeled because of its negligible radiative impact upon validations.

Figures 5a through 5d show a typical ASTI spectrum and the associated residuals with LBLRTM over the spectral range 2700 cm^{-1} to 10000 cm^{-1}. Figure 6 is an expanded view of the 7400 cm^{-1} to 7500 cm^{-1} region, whereby both the observed data and the model results have been oversampled ten times. It is noted that while some spectral lines match well in the region from 7400 cm^{-1} to 7500 cm^{-1}, others do not, both in line widths and intensities. It should be noted that these differences are not correlated with solar lines.

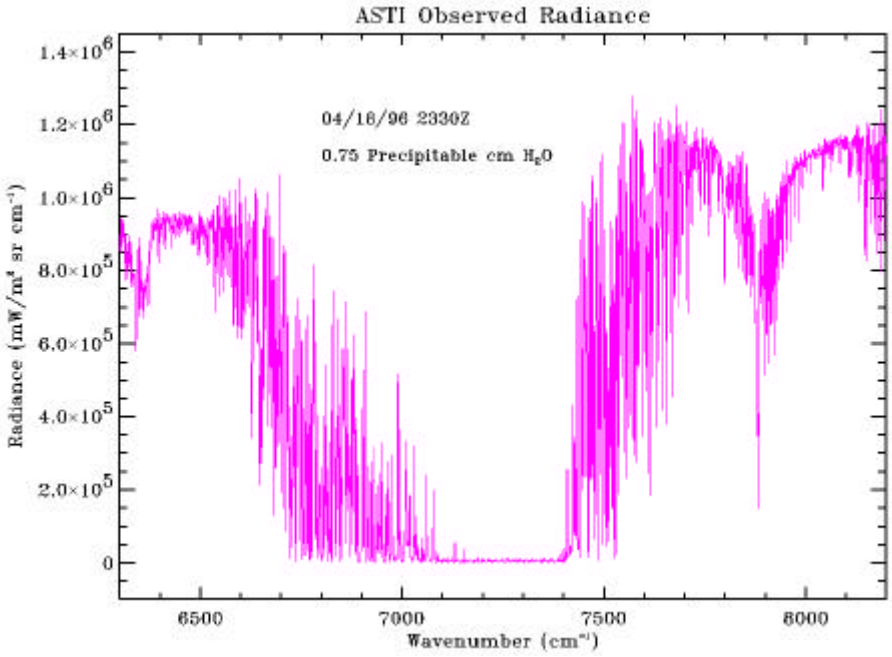

Figure 5a. ASTI observation (top) and Observed - Calculated residuals (bottom) for a representative case over the spectral range 2700 cm^{-1} to 4700 cm^{-1}. (For a color version of this figure, please see *http://www.arm.gov/docs/documents/technical/conf_9803/brown-98.pdf*.)

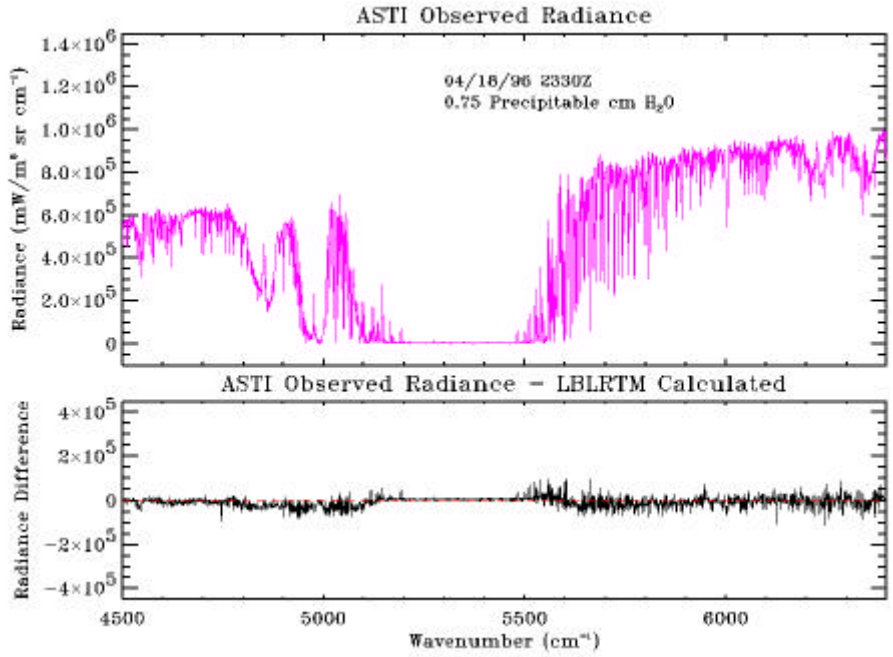

Figure 5b. ASTI observation (top) and Observed - Calculated residuals (bottom) for a representative case over the spectral range 4500 cm^{-1} to 6400 cm^{-1}. (For a color version of this figure, please see *http://www.arm.gov/docs/documents/technical/conf_9803/brown-98.pdf*.)

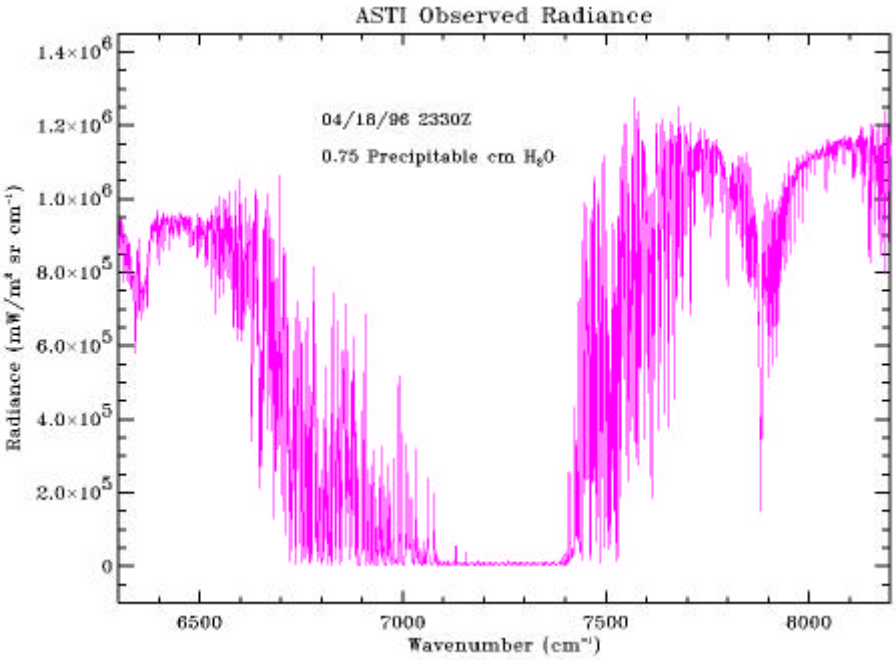

Figure 5c. ASTI observation (top) and Observed - Calculated residuals (bottom) for a representative case over the spectral range 6300 cm^{-1} to 8200 cm^{-1}. (For a color version of this figure, please see *http://www.arm.gov/docs/documents/technical/conf_9803/brown-98.pdf*.)

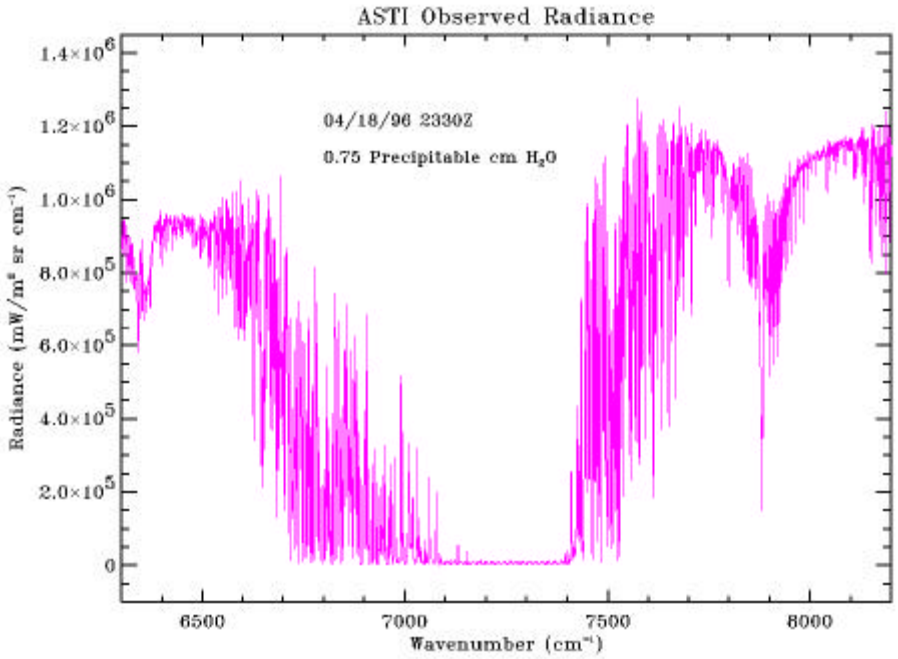

Figure 5d. ASTI observation (top) and Observed - Calculated residuals (bottom) for a representative case over the spectral range 8000 cm^{-1} to 10000 cm^{-1}. (For a color version of this figure, please see *http://www.arm.gov/docs/documents/ technical/conf_9803/brown-98.pdf*.)

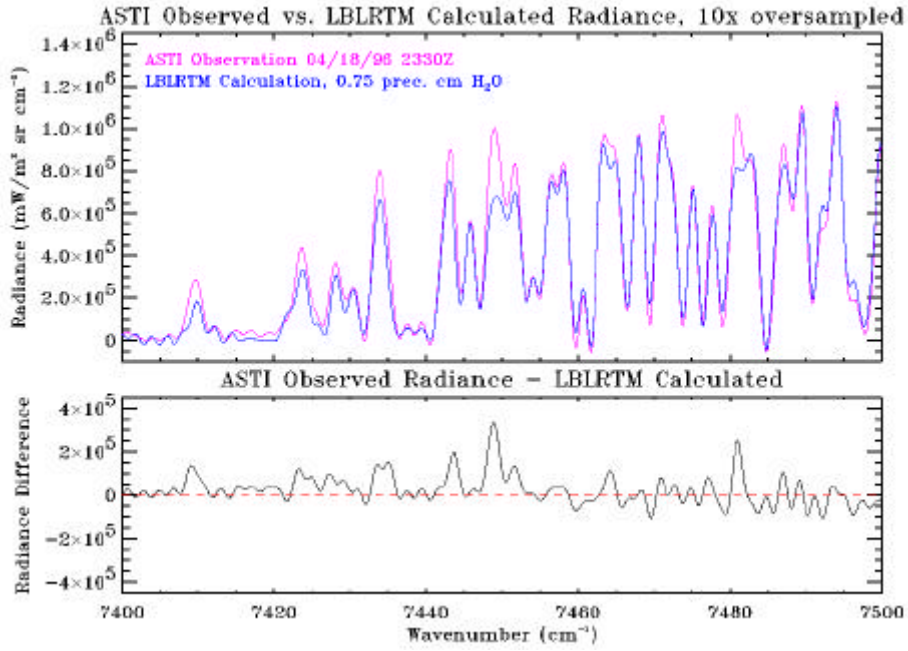

Figure 6. Oversampled ASTI observed (red) and LBLRTM calculated (blue) radiances (10x) from 7400 cm^{-1} to 7500 cm^{-1} (top) and the associated differences (bottom). (For a color version of this figure, please see *http://www.arm.gov/docs/documents/ technical/conf_9803/brown-98.pdf*.)

This suggests errors in the line list for some lines and the need to improve the representation of the instrument line shape. Further investigations are ongoing to study these differences.

The validations for all three cases show remarkable agreement between measurement and model for substantially different solar zenith angles and column water vapor amounts. Table 2 shows that, after scaling all three cases, the error in calculated instantaneous hemispherical flux at the surface is less than 1 W/m^2.

Table 2. Validation results of the initial three cases. The "Calculated Instantaneous Hemispherical Flux" column lists the spectrally integrated flux for the direct beam reaching the surface as well as the calculated downwelling flux at the top of the atmosphere (in brackets).

Case #	H_2O (prec cm)	Solar Zenith (degrees)	Calculated Instantaneous Hemis. Flux (W/m^2)	Obs – Calc (W/m^2)
1	0.60	31.0	266.76 [349.35]	-0.74
2	0.75	71.5	85,89 [129.32]	-0.73
3	3.30	27.9	233.55 [360.19]	0.30

Summary

Initial validations between ASTI-observed radiance in the direct beam and LBLRTM model results have been quite good, yielding differences less than 1 W/m^2 in instantaneous hemispherical flux from 2000 cm^{-1} to 10000 cm^{-1}. Issues associated with FOV effects in the instrument spectral calibration, O_2 collision-induced continuum bands, and Rayleigh scattering have been identified and are being addressed. Issues remain concerning spectral line parameters, instrument radiometric calibration, and solar source function errors. Over the spectral coverage of the AERI and ASTI instruments from 550 cm^{-1} to 10000 cm^{-1}, there is no evidence of water vapor dimers, water vapor clusters, or other significant unexplained gaseous absorption. These validations demonstrate the need for high resolution comparisons to identify and resolve issues of importance in the near infrared wavelengths. The QME will be extended into visible wavelengths and include diffuse irradiance validations using the RSS and the solar spectral flux radiometer (SSFR; Rabbette and Pilewskie 1998).

Acknowledgments

The authors gratefully acknowledge the support of the U.S. Department of Energy, Environmental Sciences Division, under Grant No. DE-FG02-90ER61064 and the University of Wisconsin, under Subgrant No. G02-77285.

References

Arking, A., 1996: Absorption of solar energy in the atmosphere: Discrepancy between model and observations. *Science*, **273**, 779-782.

Cess, R. D., M. H. Zhang, P. Minnis, L. Corsetti, E. G. Dutton, B. W. Forgan, D. P. Garber, W. L. Gates, J. J. Hack, E. F. Harrison, X. Jing, J. T. Kiehl, C. N. Long, J.-J. Morcrette, G. L. Potter, V. Ramanathan, B. Subasilar, C. H. Whitlock, D. F. Young, and Y. Zhou, 1995: Absorption of solar radiation by clouds: Observations versus models. *Science*, **267**, 496-499.

Harrison, L., J. J. Michalsky, and J. Berndt, 1994: The automated multi-filter rotating shadowband radiometer: An instrument for optical depth and radiation measurements. *Applied Optics*, **32**, 5118-5125.

Harrison, L., J. J. Michalsky, Q. Min, and M. Beauharnois, 1998: Analysis of rotating shadowband spectroradiometer (RSS) data. This proceedings.

Kurucz, R. L., 1992: Synthetic infrared spectra, Infrared Solar Physics, IAU Symp. 154, edited by D. M. Rabin and J. T. Jefferies, Kluwer, Acad., Norwell, Massachusetts.

Li, Z., and L. Moreau, 1996: Alteration of atmospheric solar radiation by clouds: Simulation and observation. *J. Appl. Meteorol*., **35**, 653-670.

Mlawer, E. J., S. A. Clough, P. D. Brown, T. S. Stephen, J. C. Landry, A. Goldman, and F. J. Murcray, 1998: Observed atmospheric collision-induced absorption in near-infrared oxygen bands. *J. Geophys. Res*., **103**, 3859-3863.

Neckel, H., and D. Labs, 1984: The solar radiation between 3300 and 125000A. *Sol. Phys*., **90**, 205-258.

Rabbette, M., and P. Pilweskie, 1998: Principal component analysis of solar spectral irradiance during the Fall 1997 shortwave intensive observation period. This proceedings.

Other Publications in Progress

Brown, P. D., S. A. Clough, R. O. Knuteson, H. E. Revercomb, W. L. Smith, D. Turner, T. R. Shippert, and N. E. Miller, 1998: High resolution spectral validations in the infrared: Implications for improvements to modeling, measurements, and atmospheric state specification, in preparation.